

# Intertemporal Hedging Demand under Epstein–Zin Preferences in a Multi-Asset Long-Run Risk Model: Evidence from Projected Pontryagin-Guided Deep Policy Optimization

Wonchan Cho

December 18, 2025

## Abstract

I study intertemporal hedging demand in a continuous-time multi-asset long-run risk (LRR) model under Epstein–Zin (EZ) recursive preferences. The investor trades a risk-free asset and several risky assets whose drifts and volatilities depend on an Ornstein–Uhlenbeck type LRR factor. Preferences are described by EZ utility with risk aversion  $R$ , elasticity of intertemporal substitution  $\psi$ , and discount rate  $\delta$ , so that the standard time-additive CRRA case appears as a limiting benchmark.

To handle the high-dimensional consumption–investment problem, I use a projected Pontryagin-guided deep policy optimization (P-PGDPO) scheme adapted to EZ preferences. The method starts from the continuous-time Hamiltonian implied by the Pontryagin maximum principle, represents the value and costate processes with neural networks, and updates the policy along the Hamiltonian gradient. Portfolio constraints and a lower bound on wealth are enforced by explicit projection operators rather than by adding ad hoc penalties.

Three main findings emerge from numerical experiments in a five-asset LRR economy: **(1)** the P-PGDPO algorithm achieves stable convergence across multiple random seeds, validating its reliability for solving high-dimensional EZ problems; **(2)** wealth floors materially reduce hedging demand by limiting the investor’s ability to exploit intertemporal risk-return tradeoffs; and **(3)** the learned hedging portfolios concentrate exposure in assets with high correlation to the LRR factor, confirming that EZ agents actively hedge long-run uncertainty rather than merely following myopic rules. Because EZ preferences nest time-additive CRRA in the limit  $\psi \rightarrow 1/R$ , I use CRRA as an explicit diagnostic benchmark and, when needed, a warm start to stabilize training in high dimensions.

**Keywords:** intertemporal hedging, Epstein–Zin preferences, long-run risk, dynamic portfolio choice, deep reinforcement learning, Pontryagin maximum principle

## 1 Introduction

A long-lived investor who cares about both current consumption and distant future wealth usually does more than just chase the highest instantaneous Sharpe ratio. When investment opportunities move slowly over time and macro or volatility shocks are highly persistent, it becomes natural to tilt the portfolio toward assets that hedge against future changes in the investment environment. This intertemporal hedging motive has been part of the core story in dynamic portfolio choice since [Merton \(1969, 1971\)](#), and it plays a central role in work on long-run risk and term-structure models (e.g. [Campbell and Viceira, 2002](#); [Bansal and Yaron, 2004](#)). Yet, once we leave the comfort zone of homothetic CRRA preferences and low-dimensional state variables, it quickly becomes difficult to say something concrete about the size and shape of hedging demand.

In this paper I study intertemporal hedging in a continuous-time multi-asset long-run risk (LRR) setting under Epstein–Zin (EZ) recursive preferences. The investor trades a risk-free asset

and several risky assets whose drifts and volatilities are driven by a persistent Ornstein–Uhlenbeck type LRR factor. Preferences are described by EZ utility with risk aversion  $R$ , elasticity of intertemporal substitution  $\psi$ , and discount rate  $\delta$ . This combination of a multi-asset LRR environment and EZ preferences is rich enough to generate nontrivial hedging motives, but it also means that closed-form solutions are essentially out of reach once we allow for more than a handful of assets and a realistically persistent state process.

Because explicit solutions are out of reach, I turn to a numerical approach that is still anchored in continuous-time optimality conditions. I build on the projected Pontryagin-guided deep policy optimization (P-PGDPO) framework, originally developed for time-additive preferences, and adapt it to the EZ setting. The starting point is the continuous-time Hamiltonian implied by the Pontryagin maximum principle. The value function and the associated costate process are represented by neural networks, and the portfolio and consumption rules are updated along the Hamiltonian gradient. Instead of treating portfolio constraints and wealth safety as soft penalties in the objective, I enforce them through explicit projection operators, so that every policy update remains admissible by construction. Because projections can introduce bias when constraints bind, I explicitly track how often the portfolio and consumption projections are active and report binding rates across random seeds. I also include ablations that compare projection-based enforcement with softer alternatives, so that the economic conclusions about hedging demand are not an artifact of the constraint-handling mechanism.

The main goal is not to propose yet another generic reinforcement learning algorithm, but to understand what the EZ version of the long-run risk model implies for intertemporal hedging in a concrete multi-asset environment. To that end, I focus on a five-asset LRR specification and compare the learned EZ policy to the analytic myopic (Merton-style) portfolio that ignores future changes in the investment opportunity set. The difference between the two portfolios is interpreted as an intertemporal hedging component, and I study how this component behaves across wealth and the LRR state.

Three aspects of the results are worth highlighting. First, the EZ-adapted P-PGDPO scheme can be trained in a stable way even when the state space includes both wealth and a persistent LRR factor, and when the control includes consumption and a multi-asset portfolio vector subject to constraints. Second, the learned portfolio exhibits a strongly state-dependent hedging demand: contour plots over wealth and the LRR state reveal shapes that cannot be replicated by any static combination of myopic positions. Third, the trained policy respects a lower bound on wealth while delivering economically meaningful welfare improvements and robust terminal-wealth distributions across seeds, which makes the economic trade-off between growth and safety visible in a way that is hard to obtain analytically in this setting.

**Contribution.** The paper makes two main contributions. **First**, on the *methodological* side, it demonstrates that projection-based constraint enforcement combined with Pontryagin-guided policy updates can successfully train EZ policies in continuous-time settings with multiple risky assets and persistent state variables, where both HJB and adjoint BSDE residuals must be jointly minimized. The transparent handling of constraints via projection operators—rather than via penalty terms—makes it straightforward to diagnose when binding constraints might confound the economic interpretation of hedging demand. Ablation studies confirm that the algorithm’s stability does not rely on ad hoc tuning.

**Second**, on the *economic* side, the paper provides concrete quantitative evidence that intertemporal hedging under EZ preferences is strongly state-dependent and systematically different from myopic (Merton-style) rules. In particular, hedging demand concentrates in assets with high exposure to the long-run risk factor, consistent with the idea that forward-looking agents actively manage their exposure to slowly moving shifts in the investment opportunity set. Furthermore, wealth floors—which mimic realistic solvency or borrowing constraints—materially reduce hedging activity near the boundary, a result that highlights how institutional or regulatory

constraints can limit the scope for sophisticated dynamic strategies.

Viewed this way, the paper contributes a small but concrete step toward using continuous-time, Pontryagin-guided deep learning tools to study portfolio choice with recursive preferences and long-run risk in more realistic multi-asset settings. The focus throughout is on keeping the link to the underlying stochastic control problem explicit, so that the numerical results can be read as a quantitative complement to the existing theory rather than as a black-box prediction from a generic neural network model.

This benchmarking perspective is also helpful on the computational side, where recursive objectives can be harder to optimize reliably. Formally, EZ collapses to time-additive CRRA when  $\psi = 1/R$ , so the CRRA specification serves two roles in this paper. First, it provides an economically interpretable reference point for separating genuinely recursive (intertemporal) hedging motives from purely myopic risk-taking. Second, it provides a numerically stable anchor: a CRRA-limit policy can be used to warm-start training when the fully recursive objective is difficult to optimize from scratch in higher dimensions.

## 2 Model and Preferences

### 2.1 Market

I work on a continuous-time economy over a finite horizon  $[0, T]$  on a filtered probability space  $(\Omega, \mathcal{F}, (\mathcal{F}_t)_{t \in [0, T]}, \mathbb{P})$  that supports a standard Brownian motion. Time is continuous and measured in years.

There is one risk-free asset  $B_t$  and  $d$  risky assets  $S_t^1, \dots, S_t^d$ . The risk-free asset evolves according to

$$\frac{dB_t}{B_t} = r dt, \quad (2.1)$$

where  $r \geq 0$  is a constant short rate.

Investment opportunities are driven by a persistent long-run risk (LRR) factor  $Y_t$ . I model  $Y_t$  as an Ornstein–Uhlenbeck process

$$dY_t = \kappa_y (\bar{y} - Y_t) dt + \xi dW_t^Y, \quad (2.2)$$

where  $\kappa_y > 0$  is the speed of mean reversion,  $\bar{y}$  is the long-run mean of the factor,  $\xi > 0$  is the volatility, and  $W_t^Y$  is a standard Brownian motion. The sign and magnitude of  $Y_t$  can be interpreted as capturing slowly moving macroeconomic or volatility conditions.

The  $d$  risky assets follow diffusion dynamics of the form

$$\frac{dS_t^i}{S_t^i} = \mu_i(Y_t) dt + \sum_{j=1}^m \sigma_{ij}(Y_t) dW_t^j, \quad i = 1, \dots, d, \quad (2.3)$$

where  $\mu_i(Y_t)$  is the drift of asset  $i$ ,  $\sigma_{ij}(Y_t)$  are the elements of the volatility matrix  $\sigma(Y_t) \in \mathbb{R}^{d \times m}$ , and  $W_t = (W_t^1, \dots, W_t^m)^\top$  is an  $m$ -dimensional Brownian motion. The dependence on  $Y_t$  captures time-varying expected returns and volatilities in the spirit of long-run risk models.

An investor starts at time  $t = 0$  with initial wealth  $W_0 > 0$ . At each time  $t$ , she chooses a consumption rate  $c_t \geq 0$  and a portfolio vector  $\pi_t = (\pi_t^1, \dots, \pi_t^d)^\top$ , where  $\pi_t^i$  denotes the (possibly leverage-adjusted) fraction of wealth invested in risky asset  $i$  at time  $t$ . The remaining fraction  $1 - \mathbf{1}^\top \pi_t$  is invested in the risk-free asset, where  $\mathbf{1}$  denotes a  $d$ -dimensional vector of ones.

Given a control  $(\pi_t, c_t)_{t \in [0, T]}$ , wealth evolves according to

$$dW_t = \left[ rW_t + \left( \mu(Y_t) - r\mathbf{1} \right)^\top (\pi_t W_t) - c_t \right] dt + W_t \pi_t^\top \sigma(Y_t) dW_t, \quad (2.4)$$

where  $\mu(Y_t) = (\mu_1(Y_t), \dots, \mu_d(Y_t))^\top$  and  $\sigma(Y_t)$  is the volatility matrix from (2.3). I will often write the state process as  $X_t = (W_t, Y_t)$  and the control as  $u_t = (\pi_t, c_t)$ .

The investor faces simple portfolio and wealth constraints. First, portfolio weights are required to stay in a compact admissible set  $\Pi \subset \mathbb{R}^d$ , which can encode long-only, leverage, or concentration limits. In the numerical experiments below,  $\Pi$  is chosen to represent a long-only, fully invested portfolio with a mild leverage cap. Second, wealth is required to stay above a lower bound  $W_{\min} > 0$ ,

$$W_t \geq W_{\min} \quad \text{for all } t \in [0, T], \quad (2.5)$$

which I enforce in the learning algorithm via an explicit projection step. Admissible strategies are progressively measurable processes  $(\pi_t, c_t)$  taking values in  $\Pi \times [0, \infty)$  such that the SDE (2.4) admits a unique strong solution and (2.5) is satisfied.

## 2.2 Preferences

The investor cares about the entire consumption path and terminal wealth over  $[0, T]$ . I use two preference specifications that share the same primitive parameters but differ in how they aggregate risk and intertemporal trade-offs: a time-additive CRRA benchmark and Epstein–Zin recursive utility.

### CRRA benchmark

As a starting point, consider a standard time-additive CRRA specification. Let  $R > 0$  denote relative risk aversion and  $\delta > 0$  the subjective discount rate. Instantaneous utility from consumption is

$$u(c) = \begin{cases} \frac{c^{1-R}}{1-R}, & R \neq 1, \\ \log c, & R = 1. \end{cases} \quad (2.6)$$

For given admissible controls  $(\pi_t, c_t)$ , the CRRA value functional is

$$J^{\text{CRRA}}(W_0, Y_0; \pi, c) = \mathbb{E} \left[ \int_0^T e^{-\delta t} u(c_t) dt + e^{-\delta T} \varphi(W_T) \right], \quad (2.7)$$

where  $\varphi(\cdot)$  is a terminal utility function, typically of the same CRRA form as  $u(\cdot)$ . The CRRA optimal control problem is

$$V^{\text{CRRA}}(W_0, Y_0) = \sup_{(\pi, c) \text{ admissible}} J^{\text{CRRA}}(W_0, Y_0; \pi, c). \quad (2.8)$$

In simple one-asset settings with constant investment opportunities, this problem admits closed-form solutions of Merton type. In the multi-asset LRR setting described above, closed forms quickly become unwieldy, but the CRRA problem remains a useful benchmark.

### Epstein–Zin recursive preferences

To separate risk aversion from the elasticity of intertemporal substitution (EIS), I use Epstein–Zin (EZ) recursive utility. The primitive parameters are now

$$R > 0 \quad (\text{risk aversion}), \quad \psi > 0 \quad (\text{EIS}), \quad \delta > 0 \quad (\text{discount rate}).$$

In discrete time, EZ preferences can be written via the familiar aggregator (see, e.g., [Epstein and Zin \(1989\)](#)) that nests time-additive CRRA as a special case. In continuous time, the same structure leads to a value process  $V_t$  that solves a nonlinear HJB or BSDE representation. Informally,  $V_t$  trades off current consumption and the continuation value  $V_{t+dt}$  in a way that depends on both  $R$  and  $\psi$ , so that attitudes toward risk and intertemporal substitution are no longer tied by the restriction  $\psi = 1/R$ .

Rather than work directly with the BSDE form here, I take the usual continuous-time EZ specification used in the long-run risk literature and use it to derive the Hamiltonian and Pontryagin first-order conditions that underlie the learning algorithm. The key point for this paper is that:

- when  $\psi = 1/R$ , EZ preferences collapse to the time-additive CRRA case, so CRRA remains a natural limiting benchmark, and
- when  $\psi \neq 1/R$ , the investor's risk aversion  $R$  and EIS  $\psi$  enter the Hamiltonian in different ways, which generates richer intertemporal hedging motives in the LRR setting.

In Section 3 below, I spell out how the EZ aggregator enters the continuous-time Hamiltonian, how the associated costate process is parameterized, and how the Pontryagin conditions are turned into a projected deep policy optimization scheme.

**Why report both CRRA and EZ benchmarks?** Even when the primary objective is Epstein–Zin welfare, reporting CRRA-side quantities is useful. The CRRA limit provides a transparent baseline that isolates the incremental role of recursive preferences. It also offers a disciplined implementation check: when  $\psi$  is chosen near  $1/R$ , the EZ-P-PGDPO solution should approach the CRRA behavior, which acts as a robustness and debugging diagnostic in high-dimensional settings.

### 2.3 Control problem and EZ value representation

We collect the relevant state variables in

$$X_t = (W_t, Y_t)^\top \in \mathcal{X} \subset \mathbb{R}^2,$$

where  $W_t$  denotes financial wealth and  $Y_t$  is the long-run risk state. The control at time  $t$  is

$$u_t = (\pi_t, c_t) \in \mathcal{U}(X_t),$$

where  $\pi_t \in \mathbb{R}^d$  is the vector of portfolio weights on the  $d$  risky assets (in dollar or fraction form, depending on the parametrization) and  $c_t \geq 0$  is the consumption rate. The admissible control set  $\mathcal{U}(x)$  encodes the leverage and consumption caps as well as the wealth floor constraint, see Section 2.

The joint dynamics of  $(W_t, Y_t)$  can be written in compact form as

$$dX_t = b(t, X_t, u_t) dt + \sigma(t, X_t, u_t) dB_t, \quad t \in [0, T], \quad (2.9)$$

where  $B_t$  is a Brownian motion of appropriate dimension,  $b(\cdot)$  collects the drifts of wealth and the long-run risk factor, and  $\sigma(\cdot)$  collects their diffusion coefficients. The associated infinitesimal generator under a fixed control  $u$  is

$$\mathcal{L}^u \varphi(t, x) = \partial_t \varphi(t, x) + b(t, x, u)^\top \nabla_x \varphi(t, x) + \frac{1}{2} \text{Tr}(\sigma(t, x, u) \sigma(t, x, u)^\top D_x^2 \varphi(t, x)), \quad (2.10)$$

for smooth test functions  $\varphi$ .

**Epstein–Zin aggregator.** For given preference parameters  $(R, \psi, \delta)$  with  $R > 0$ ,  $R \neq 1$ ,  $\psi > 0$ ,  $\psi \neq 1$ , the one-period EZ aggregator is given by

$$f^{\text{EZ}}(c, v) = \delta \theta v \left[ \left( \frac{c}{((1-R)v)^{1/(1-R)}} \right)^{1-S} - 1 \right], \quad S = \frac{1}{\psi}, \quad \theta = \frac{1-R}{1-S}, \quad (2.11)$$

for current consumption  $c$  and continuation value  $v$ . As discussed above, in the limit  $\psi \rightarrow 1/R$  this aggregator collapses to the usual CRRA form with instantaneous utility  $u(c) = c^{1-R}/(1-R)$ .

**Value function and dynamic programming.** Given an admissible control  $u$ , let  $J(t, x; u)$  denote the Epstein–Zin continuation value at time  $t$  starting from state  $X_t = x$  and following  $u$  thereafter. We define the value function

$$V(t, x) = \sup_{u \in \mathcal{U}} J(t, x; u), \quad (t, x) \in [0, T] \times \mathcal{X},$$

where the supremum is over progressively measurable controls taking values in  $\mathcal{U}(X_t)$  and satisfying the wealth floor and integrability conditions.

At an informal level, the dynamic programming principle (DPP) states that for any small  $h > 0$ ,

$$V(t, x) = \sup_{u \in \mathcal{U}} \mathbb{E} \left[ V(t+h, X_{t+h}^{t,x;u}) + \int_t^{t+h} f^{\text{EZ}}(c_s, V(s, X_s^{t,x;u})) \, ds \right], \quad (2.12)$$

where  $X^{t,x;u}$  denotes the state starting from  $X_t = x$  controlled by  $u$ . Dividing (2.12) by  $h$  and letting  $h \rightarrow 0$ , and applying Itô’s formula to  $V(s, X_s^{t,x;u})$ , leads to the Hamilton–Jacobi–Bellman (HJB) equation

$$0 = \partial_t V(t, x) + \sup_{u \in \mathcal{U}(x)} \left\{ f^{\text{EZ}}(c, V(t, x)) + \tilde{\mathcal{L}}^u V(t, x) \right\}, \quad (t, x) \in [0, T) \times \mathcal{X}, \quad (2.13)$$

with appropriate terminal/boundary conditions at  $t = T$  and on the wealth band. Here  $\tilde{\mathcal{L}}^u$  denotes the spatial part of the generator,

$$\tilde{\mathcal{L}}^u V = b(t, x, u)^\top \nabla_x V(t, x) + \frac{1}{2} \text{Tr}(\sigma(t, x, u) \sigma(t, x, u)^\top D_x^2 V(t, x)).$$

**BSDE representation.** In a Markovian setting such as the long–run risk model above, the HJB equation (2.13) admits a backward stochastic differential equation (BSDE) representation. Formally, along an optimal state–control pair  $(X_t^*, u_t^*)$ , the EZ value process  $V_t = V(t, X_t^*)$  and an associated  $\mathbb{R}^m$ –valued process  $Z_t$  solve

$$-dV_t = f^{\text{EZ}}(c_t^*, V_t) \, dt - Z_t^\top dB_t, \quad V_T = G(X_T^*), \quad (2.14)$$

for some terminal condition  $G$ . Conversely, under regularity conditions, the solution of (2.14) recovers the HJB value function via  $V_t = V(t, X_t^*)$ . This BSDE viewpoint is the starting point for our value network approximation and for the loss (3.16) used in the P–PGDPO algorithm.

### 3 P–PGDPO algorithm for EZ preferences

#### 3.1 From HJB and Pontryagin conditions to the losses

The P–PGDPO algorithm is built to approximately satisfy the HJB/BSDE system (2.13)–(2.14) and the associated Pontryagin maximum principle along simulated trajectories. To make this connection explicit, we first recall the compact state dynamics (2.9),

$$dX_t = b(t, X_t, u_t) \, dt + \sigma(t, X_t, u_t) \, dB_t,$$

and the EZ aggregator  $f^{\text{EZ}}$ . We then introduce a Hamiltonian that combines the running aggregator with the controlled drift:

$$H(t, x, u, \lambda; V) = f^{\text{EZ}}(c, V(t, x)) + \lambda^\top b(t, x, u), \quad (3.1)$$

where  $\lambda \in \mathbb{R}^2$  plays the role of a costate and  $V$  is the value function. In the classical stochastic maximum principle, an optimal triple  $(X_t^*, \lambda_t^*, u_t^*)$  satisfies the state equation, the backward costate equation, and a stationarity condition:

$$\text{state: } dX_t^* = b(t, X_t^*, u_t^*) \, dt + \sigma(t, X_t^*, u_t^*) \, dB_t, \quad (3.2)$$

$$\text{costate: } d\lambda_t^* = -\nabla_x H(t, X_t^*, u_t^*, \lambda_t^*; V) \, dt + \Gamma_t \, dB_t, \quad (3.3)$$

$$\text{stationarity: } 0 \in \partial_u H(t, X_t^*, u_t^*, \lambda_t^*; V) + N_{\mathcal{U}(X_t^*)}(u_t^*), \quad (3.4)$$

where  $\Gamma_t$  is a suitable adapted process and  $N_{\mathcal{U}(x)}(u)$  denotes the normal cone of the constraint set  $\mathcal{U}(x)$  at  $u$ . The costate can be interpreted as a generalized gradient of the value function, in the sense that under regularity assumptions  $\lambda_t^* = \nabla_x V(t, X_t^*)$ .

In the EZ setting the HJB equation and the Pontryagin system are coupled through the aggregator  $f^{\text{EZ}}$  and the wealth floor constraint. Rather than solving (2.13)–(3.4) analytically, we parameterize the value, costate, and control by neural networks

$$V_\theta(t, x), \quad \lambda_\eta(t, x), \quad u_\phi(t, x),$$

and enforce approximate satisfaction of the BSDE, gradient consistency, and stationarity relations along simulated trajectories. This yields three complementary objective functionals: a value consistency loss, a costate consistency loss, and a Hamiltonian ascent objective.

**Value loss (BSDE consistency).** Given a simulated path  $\{(t_k, X_{t_k}, u_k, c_k)\}_{k=0}^N$  under a candidate policy  $u_\phi$ , we define the discrete BSDE residual by

$$R_k^{\text{val}} = V_\theta(t_k, X_{t_k}) - V_\theta(t_{k+1}, X_{t_{k+1}}) - f^{\text{EZ}}(c_k, V_\theta(t_k, X_{t_k})) \Delta t, \quad k = 0, \dots, N-1.$$

The value loss aggregates these residuals in mean square:

$$\mathcal{L}_{\text{val}}(\theta, \phi) = \mathbb{E} \left[ \sum_{k=0}^{N-1} (R_k^{\text{val}})^2 \right], \quad (3.5)$$

where the expectation is approximated by Monte Carlo over simulated paths. Minimizing  $\mathcal{L}_{\text{val}}$  encourages  $V_\theta$  to approximate the EZ value process along the trajectories generated by  $u_\phi$ .

**Adjoint loss (gradient consistency).** The costate network  $\lambda_\eta$  is meant to approximate the spatial gradient of the value network. Inspired by the identity  $\lambda_t^* = \nabla_x V(t, X_t^*)$ , we define

$$\mathcal{L}_{\text{adj}}(\theta, \eta) = \mathbb{E} \left[ \sum_{k=0}^N \|\lambda_\eta(t_k, X_{t_k}) - \nabla_x V_\theta(t_k, X_{t_k})\|^2 \right]. \quad (3.6)$$

This loss ties the two networks together and provides a differentiable approximation of the costate needed to guide the policy gradient.

**Actor objective (Hamiltonian ascent with projection).** Finally, for a fixed pair  $(\theta, \eta)$ , the policy parameters  $\phi$  are updated to ascend the Hamiltonian evaluated along the simulated trajectories. We consider the objective

$$J_{\text{act}}(\phi; \theta, \eta) = \mathbb{E} \left[ \sum_{k=0}^{N-1} H(t_k, X_{t_k}, u_\phi(t_k, X_{t_k}), \lambda_\eta(t_k, X_{t_k}); V_\theta) \right] - \beta \mathcal{R}(\phi), \quad (3.7)$$

where  $\mathcal{R}(\phi)$  is a regularization term (for example, penalizing leverage, large consumption ratios, or deviation from a baseline policy) and  $\beta > 0$  is a penalty weight. The control  $u_\phi(t_k, X_{t_k})$  is passed through the projection operator enforcing the wealth floor and leverage/consumption caps, so that the effective control lies in  $\mathcal{U}(X_{t_k})$ . In the continuous-time limit, the gradient of  $J_{\text{act}}$  with respect to  $\phi$  recovers a Pontryagin-guided policy gradient direction aligned with the stationarity condition (3.4).

In practice, the overall P-PGDPO update alternates between: (i) minimizing  $\mathcal{L}_{\text{val}}$  and  $\mathcal{L}_{\text{adj}}$  with respect to  $(\theta, \eta)$ , and (ii) maximizing  $J_{\text{act}}$  with respect to  $\phi$ , using stochastic gradient steps on mini-batches of simulated trajectories.

### 3.2 Hamiltonian and Pontryagin conditions (EZ case)

To connect the HJB representation (2.13) with the P-PGDPO algorithm, it is convenient to rewrite the control problem in terms of a Hamiltonian and the associated costate (adjoint) process.

**Compact state dynamics.** Recall the compact notation

$$dX_t = b(X_t, u_t) dt + \sigma(X_t, u_t) dB_t,$$

where  $X_t \in \mathbb{R}^{1+m}$  and  $u_t \in \mathcal{U}$ . We also keep the EZ value process  $V_t$  defined by (2.14).

**Hamiltonian.** Given a state  $x$ , an EZ continuation value  $v$ , a control  $u$ , and a costate vector  $p \in \mathbb{R}^{1+m}$ , the *running* Hamiltonian associated with the EZ problem is

$$H^{\text{EZ}}(t, x, v, p, u) := f^{\text{EZ}}(c, v) + p^\top b(x, u), \quad (3.8)$$

where  $c$  is the consumption component of  $u$ .

**Costate (adjoint) dynamics.** Formally, suppose the value function  $V(t, x)$  is smooth and define the costate process along a controlled trajectory by

$$\lambda_t := \nabla_x V(t, X_t) \in \mathbb{R}^{1+m}. \quad (3.9)$$

Then Itô's formula and the HJB equation imply that  $\lambda_t$  solves the backward SDE

$$d\lambda_t = -\partial_x H^{\text{EZ}}(t, X_t, V(t, X_t), \lambda_t, u_t) dt + \Xi_t^\top dB_t, \quad \lambda_T = \partial_x U(W_T), \quad (3.10)$$

for some adapted process  $\Xi_t$ . Because the bequest utility  $U$  depends only on wealth, the terminal condition has the simple form

$$\lambda_T = (U'(W_T), 0, \dots, 0)^\top.$$

**Pontryagin maximum principle.** A control  $u^* = (\pi^*, c^*)$  with corresponding state  $X^*$ , value process  $V^*$ , and costate  $\lambda^*$  is (locally) optimal only if it satisfies

$$dX_t^* = b(X_t^*, u_t^*) dt + \sigma(X_t^*, u_t^*) dB_t, \quad X_0^* = x_0, \quad (3.11)$$

$$d\lambda_t^* = -\partial_x H^{\text{EZ}}(t, X_t^*, V^*(t, X_t^*), \lambda_t^*, u_t^*) dt + \Xi_t^{*\top} dB_t, \quad \lambda_T^* = \partial_x U(W_T^*), \quad (3.12)$$

$$0 = \partial_u H^{\text{EZ}}(t, X_t^*, V^*(t, X_t^*), \lambda_t^*, u_t^*), \quad \text{for a.e. } t \in [0, T], \quad (3.13)$$

together with appropriate transversality and admissibility conditions. The stationarity condition (3.13) encodes the first-order optimality conditions (FOC) for both the portfolio weights  $\pi_t^*$  and consumption  $c_t^*$ .

### 3.3 Neural parameterization

The P-PGDPO algorithm replaces the unknown objects  $(V, \lambda, u)$  in (3.11)–(3.13) by neural networks.

**Inputs and outputs.** At each time  $t \in [0, T]$  the observable state is

$$s_t := (t, X_t) = (t, W_t, Y_t).$$

Based on this state, three networks are evaluated:

- **Value network**  $V_\theta : \mathcal{S} \rightarrow \mathbb{R}$  returns an approximation of  $V(t, x)$ .
- **Costate network**  $\lambda_\eta : \mathcal{S} \rightarrow \mathbb{R}^{1+m}$  returns an approximation of  $\nabla_x V(t, x)$ .
- **Policy network**  $\tilde{u}_\phi : \mathcal{S} \rightarrow \mathbb{R}^{d+1}$  outputs an unconstrained control  $\tilde{u}_\phi(s_t) = (\tilde{\pi}_t, \tilde{c}_t)$ .

Here  $\mathcal{S}$  denotes the compact state domain used for training (time, wealth band, and long-run risk band).

**Projection to admissible controls.** The actual control used in simulation is the projection of  $\tilde{u}_\phi(s_t)$  to the admissible set:

$$u_\phi(s_t) := \mathcal{P}(\tilde{u}_\phi(s_t); W_t) = (\pi_\phi(s_t), c_\phi(s_t)) \in \Pi \times [0, \bar{c}W_t], \quad (3.14)$$

where  $\Pi$  is the portfolio constraint set and  $\bar{c}$  is an upper bound on the consumption ratio. The projection operator  $\mathcal{P}$  is defined explicitly in Section 3.5.

All three networks are implemented as fully connected feedforward architectures with shared input  $(t, W, Y)$  and separate parameters  $\theta, \eta, \phi$ . Depth and width are kept moderate (three to four hidden layers) to balance approximation power and stability.

### 3.4 Loss functions

Training proceeds by simulating mini-batches of trajectories under the current projected policy  $u_\phi$  and minimizing three losses that mirror the structure of the EZ–PMP system: (i) a value (BSDE) consistency loss, (ii) a costate consistency loss, and (iii) a Hamiltonian ascent (policy) loss.

Let  $0 = t_0 < t_1 < \dots < t_N = T$  be a time grid with step  $\Delta t := t_{k+1} - t_k$ . A mini-batch consists of simulated paths  $\{(X_{t_k}^{(n)}, u_{t_k}^{(n)})_{k=0, \dots, N}\}_{n=1}^M$  under the current policy.

**Value (BSDE) consistency loss.** The continuous-time EZ BSDE (2.14) implies, in discrete time,

$$V(t_k, X_{t_k}) \approx V(t_{k+1}, X_{t_{k+1}}) + f^{\text{EZ}}(c_{t_k}, V(t_k, X_{t_k})) \Delta t. \quad (3.15)$$

Replacing  $V$  by  $V_\theta$  and taking a squared residual gives the value loss

$$\mathcal{L}_{\text{val}}(\theta) := \frac{1}{MN} \sum_{n=1}^M \sum_{k=0}^{N-1} \left[ V_\theta(t_k, X_{t_k}^{(n)}) - V_\theta(t_{k+1}, X_{t_{k+1}}^{(n)}) - f^{\text{EZ}}(c_{t_k}^{(n)}, V_\theta(t_k, X_{t_k}^{(n)})) \Delta t \right]^2. \quad (3.16)$$

The terminal condition  $V(T, x) = U(w)$  is enforced by replacing  $V_\theta(t_N, X_{t_N}^{(n)})$  with  $U(W_{t_N}^{(n)})$  in the last time step.

**Costate consistency loss.** By construction the costate should satisfy  $\lambda_t = \nabla_x V(t, X_t)$ . We encourage this by introducing the gradient-matching loss

$$\mathcal{L}_{\text{adj}}(\theta, \eta) := \frac{1}{MN} \sum_{n=1}^M \sum_{k=0}^N \left\| \lambda_\eta(t_k, X_{t_k}^{(n)}) - \nabla_x V_\theta(t_k, X_{t_k}^{(n)}) \right\|^2, \quad (3.17)$$

where the gradient  $\nabla_x V_\theta$  is obtained by automatic differentiation with respect to the state input. In practice this term is important for the stability of the Hamiltonian gradient used in the policy update.

**Hamiltonian ascent (policy) loss.** Given  $V_\theta$  and  $\lambda_\eta$ , the Pontryagin stationarity condition (3.13) suggests that an optimal policy should (locally) maximize the Hamiltonian  $H^{\text{EZ}}(t, x, V_\theta, \lambda_\eta, u)$ . We therefore define the actor objective

$$J_{\text{act}}(\phi) := \frac{1}{MN} \sum_{n=1}^M \sum_{k=0}^{N-1} H^{\text{EZ}}\left(t_k, X_{t_k}^{(n)}, V_\theta(t_k, X_{t_k}^{(n)}), \lambda_\eta(t_k, X_{t_k}^{(n)}), u_\phi(t_k, X_{t_k}^{(n)})\right), \quad (3.18)$$

and perform stochastic gradient *ascent* on  $J_{\text{act}}$ . Equivalently, we define the actor loss

$$\mathcal{L}_{\text{act}}(\phi) := -J_{\text{act}}(\phi) \quad (3.19)$$

and minimize it by gradient descent.

**Total loss and updates.** The critic (value) and costate networks are trained by minimizing

$$\mathcal{L}_{\text{crit}}(\theta, \eta) := \mathcal{L}_{\text{val}}(\theta) + \lambda_{\text{adj}} \mathcal{L}_{\text{adj}}(\theta, \eta),$$

with a positive weight  $\lambda_{\text{adj}}$ . The actor network is trained by minimizing  $\mathcal{L}_{\text{act}}(\phi)$ . In the implementation, all three networks are updated jointly with Adam optimizers and separate learning rates.

### 3.5 Projection operators and wealth floor

A key feature of the P-PGDPO scheme is that portfolio and wealth constraints are enforced by explicit projection operators, not by large penalty terms in the loss. This keeps simulated trajectories admissible by construction.

**Portfolio projection.** Let  $\tilde{\pi} \in \mathbb{R}^d$  be the unconstrained output of the policy network at state  $(t, x)$ . The admissible portfolio set is the leverage-constrained simplex

$$\Pi := \{\pi \in \mathbb{R}^d : \pi_i \geq 0, \sum_{i=1}^d \pi_i \leq \ell_{\max}\}, \quad (3.20)$$

for some leverage cap  $\ell_{\max} \geq 1$ . We define the projection  $\mathcal{P}_\pi : \mathbb{R}^d \rightarrow \Pi$  by

$$\mathcal{P}_\pi(\tilde{\pi}) := \arg \min_{\pi \in \Pi} \|\pi - \tilde{\pi}\|^2. \quad (3.21)$$

This is the Euclidean projection onto a truncated simplex, for which efficient closed-form algorithms are available.

**Projection-induced bias and diagnostics.** Because projection is non-linear and may be active on a non-negligible subset of samples, the projected policy  $\Pi(\tilde{\pi}_\theta)$  can be systematically different from the unconstrained network output  $\tilde{\pi}_\theta$ . This matters for interpretation: large intertemporal ‘‘hedging’’ patterns could, in principle, be partly driven by constraints rather than by genuine state dependence in the unconstrained control.

To make this transparent, I report three projection diagnostics in all experiments: (i) the average relative projection distance  $\mathbb{E}[\|\Pi(\tilde{\pi}) - \tilde{\pi}\|_2 / (\|\tilde{\pi}\|_2 + \varepsilon)]$ , (ii) the binding rate  $\mathbb{P}(\Pi(\tilde{\pi}) \neq \tilde{\pi})$ , and (iii) the fraction of time steps at which the budget or long-only constraints are active. In the seed study, these diagnostics are aggregated as mean  $\pm$  standard deviation across seeds.

For consumption policies, binding rates below 40–50% indicate interior optimal solutions. For portfolio policies under the long-only, fully-invested constraint  $\{\pi \geq 0, \sum_i \pi_i = 1\}$ , the constraint is an equality and naturally leads to boundary solutions. To study interior portfolio policies, one can relax the equality to an inequality  $\sum_i \pi_i \leq \ell_{\max}$ , though this changes the economic interpretation (allowing cash holdings or mild leverage).

**Consumption projection.** Given current wealth  $W_t$  and an unconstrained network output  $\tilde{c}$ , the admissible consumption is

$$\mathcal{P}_c(\tilde{c}; W_t) := \min\{\max\{\tilde{c}, 0\}, \bar{c}W_t\}, \quad (3.22)$$

where  $\bar{c} \in (0, 1)$  is a pre-specified upper bound on the consumption ratio. This ensures nonnegative consumption and rules out one-off spikes that would deplete wealth in a single step.

**Wealth floor enforcement: rationale and implementation.** In all Monte Carlo rollouts used for training and evaluation, I enforce a lower wealth bound  $W_{\min} > 0$  for three reasons: (i) to avoid numerical instabilities when computing  $W^{1-R}/(1-R)$  for large  $R$ ; (ii) to ensure that the recursive utility aggregator remains well-defined when consumption approaches zero; and (iii) to represent a realistic bankruptcy constraint or minimum subsistence requirement.

*Economic interpretation.* The floor can be viewed as an exogenous borrowing constraint or a minimal wealth level below which the investor cannot operate (e.g., due to transaction costs or institutional restrictions). While stylized, this mimics real-world solvency requirements and allows us to study how binding constraints affect intertemporal hedging. Alternative implementations—such as reflecting boundaries or utility penalties for low wealth—yield qualitatively similar conclusions but complicate the costate dynamics.

Concretely, for an Euler step with time increment  $\Delta t$ , the wealth update is

$$W_{k+1} = \max\{W_{\min}, W_k(1 + r\Delta t + \pi_k^\top((\mu - r\mathbf{1})\Delta t + \Sigma\Delta B_k)) - c_k \Delta t\}. \quad (3.23)$$

I report the “floor-hit rate”  $\mathbb{P}(W_{k+1} = W_{\min})$  in all tables. In well-trained policies, this rate is typically below 5%, confirming that the floor is a safety guard rather than a perpetually binding constraint. Ablations with the floor disabled (presented in the robustness section) verify that the main hedging patterns persist, though with slightly higher variance in terminal wealth.

**Impact on hedging demand.** The presence of a wealth floor has a first-order effect on intertemporal hedging: when wealth is near  $W_{\min}$ , the investor cannot afford aggressive positions designed to hedge future shocks, since any adverse realization could trigger the floor and lock the agent at the boundary. This “hedging suppression” effect is particularly pronounced for EZ preferences with  $\psi < 1$ , where the value function is highly sensitive to downside outcomes. Consequently, we observe that hedging demand  $\pi^{\text{EZ}} - \pi^{\text{myopic}}$  declines sharply as  $W \rightarrow W_{\min}$ , a pattern confirmed by the wealth-state contour plots in Section 6.

Combining these pieces, the full projection map from (3.14) is

$$\mathcal{P}(\tilde{\pi}, \tilde{c}; W_t) := (\mathcal{P}_\pi(\tilde{\pi}), \mathcal{P}_c(\tilde{c}; W_t)). \quad (3.24)$$

### 3.6 Training algorithm

For completeness, Algorithm 1 summarizes the training loop. The main point is that the actor update is driven by the Hamiltonian gradient implied by the EZ–Pontryagin system, while constraints are enforced by projection at every step.

---

**Algorithm 1** P-PGDPO under Epstein–Zin preferences

---

- 1: **Input:** model parameters  $(r, \mu, \Sigma, \kappa, \bar{y}, \Xi)$ , EZ parameters  $(R, \psi, \delta)$ , horizon  $T$  and time grid  $(t_k)_{k=0}^N$ , wealth band  $[W_{\min}, W_{\max}]$ , portfolio set  $\Pi$  and consumption cap  $\bar{c}$ , batch size  $M$ , learning rates  $(\alpha_\theta, \alpha_\eta, \alpha_\phi)$ .
- 2: **Initialize** network parameters  $\theta, \eta, \phi$ .
- 3: **for** iteration  $= 1, 2, \dots$  **do**
- 4:     Sample initial states  $X_0^{(n)} = (W_0^{(n)}, Y_0^{(n)})$ ,  $n = 1, \dots, M$ .
- 5:     **for**  $k = 0$  to  $N - 1$  **do**
- 6:         **for**  $n = 1$  to  $M$  **do**
- 7:              $s_{t_k}^{(n)} \leftarrow (t_k, X_{t_k}^{(n)})$
- 8:              $(\tilde{\pi}_{t_k}^{(n)}, \tilde{c}_{t_k}^{(n)}) \leftarrow \tilde{u}_\phi(s_{t_k}^{(n)})$
- 9:              $(\pi_{t_k}^{(n)}, c_{t_k}^{(n)}) \leftarrow \mathcal{P}(\tilde{\pi}_{t_k}^{(n)}, \tilde{c}_{t_k}^{(n)}; W_{t_k}^{(n)})$
- 10:             Simulate  $X_{t_{k+1}}^{(n)}$  from (2.9) with control  $u_{t_k}^{(n)} = (\pi_{t_k}^{(n)}, c_{t_k}^{(n)})$  and wealth floor projection (3.23).
- 11:         **end for**
- 12:     **end for**
- 13:     Compute losses  $\mathcal{L}_{\text{val}}(\theta)$  and  $\mathcal{L}_{\text{adj}}(\theta, \eta)$  from (3.16)–(3.17).
- 14:     Update critic and costate parameters by one step of Adam on  $\mathcal{L}_{\text{crit}}(\theta, \eta)$ .
- 15:     Compute actor loss  $\mathcal{L}_{\text{act}}(\phi)$  from (3.19).
- 16:     Update actor parameters by one step of Adam on  $\mathcal{L}_{\text{act}}(\phi)$ .
- 17: **end for**
- 18: **Output:** trained networks  $(V_\theta, \lambda_\eta, u_\phi)$ .

---

### 3.7 Neural parameterization and training objective

To turn the Pontryagin conditions into a learning scheme, I parameterize three objects with neural networks:

- a value (or critic) network  $V_\theta(t, x)$ , intended to approximate the EZ value function,
- a costate network  $\Lambda_\phi(t, x)$ , intended to approximate the adjoint process  $p_t$ , and
- a policy (or actor) network  $U_\eta(t, x)$ , which outputs a candidate control  $u = (\pi, c)$  at each state  $(t, x)$ .

The training objective combines three ingredients:

- (i) a temporal consistency or Bellman-type loss that encourages  $V_\theta$  to satisfy the EZ HJB/BSDE relation along simulated trajectories,
- (ii) a Pontryagin loss that encourages  $\Lambda_\phi$  to match the gradient of  $V_\theta$  with respect to the state, so that  $\Lambda_\phi \approx \nabla_x V_\theta$ , and
- (iii) a Hamiltonian ascent term that updates the actor parameters  $\eta$  in the direction of the gradient of  $\mathcal{H}^{\text{EZ}}$  with respect to the control, evaluated at the current networks.

Concretely, I simulate mini-batches of state trajectories  $(X_t)$  under the current policy, evaluate the approximate Hamiltonian  $\mathcal{H}^{\text{EZ}}(t, X_t, V_\theta, \Lambda_\phi, U_\eta)$  along these paths, and collect gradients  $\nabla_u \mathcal{H}^{\text{EZ}}(t, x, v, p, u)$  via automatic differentiation. The actor update then takes the form

$$\eta \leftarrow \eta + \alpha_\eta \mathbb{E}[\nabla_\eta U_\eta(t, X_t) \nabla_u \mathcal{H}^{\text{EZ}}(t, X_t, V_\theta, \Lambda_\phi, U_\eta)], \quad (3.25)$$

with a learning rate  $\alpha_\eta > 0$ , followed by a projection step that enforces the portfolio and wealth constraints. The critic and costate networks are updated in parallel by minimizing their respective losses with stochastic gradient descent.

This construction keeps the link to the underlying stochastic control problem explicit: the actor is not trained to maximize an opaque cumulative reward but to move in directions that are locally consistent with the Pontryagin first-order conditions under EZ preferences.

### 3.8 Policy gradient from the EZ Pontryagin system: what is different

Our actor update is not based on a generic discrete-time RL objective (returns/advantages), but on direct Hamiltonian ascent implied by the EZ stochastic maximum principle. Recall the EZ Hamiltonian

$$H^{EZ}(t, x, v, p, u) := f^{EZ}(c, v) + p^\top b(x, u), \quad u = (\pi, c), \quad (3.26)$$

where  $f^{EZ}$  is the Epstein–Zin aggregator (A) and  $p = \nabla_x V(t, x)$  is the costate.

**Actor objective.** Given neural approximations  $(V_\theta, \lambda_\eta, \tilde{u}_\phi)$  and the projected control  $u_\phi = P(\tilde{u}_\phi)$ , we maximize the empirical Hamiltonian average

$$J_{\text{act}}(\phi) := \frac{1}{MN} \sum_{n=1}^M \sum_{k=0}^{N-1} H^{EZ}\left(t_k, X_{t_k}^{(n)}, V_\theta(t_k, X_{t_k}^{(n)}), \lambda_\eta(t_k, X_{t_k}^{(n)}), u_\phi(t_k, X_{t_k}^{(n)})\right). \quad (3.27)$$

**Deterministic policy gradient (Hamiltonian ascent).** Whenever  $P$  is differentiable at the current  $\tilde{u}_\phi(s)$ , the chain rule gives

$$\nabla_\phi J_{\text{act}}(\phi) = \mathbb{E}\left[\sum_{k=0}^{N-1} (\nabla_\phi u_\phi(s_k))^\top \nabla_u H^{EZ}(t_k, x_k, v_k, p_k, u_k)\right], \quad (3.28)$$

with  $(v_k, p_k) = (V_\theta(t_k, x_k), \lambda_\eta(t_k, x_k))$ . In particular, for the wealth drift  $b_W = rW + \pi^\top \mu(Y) - c$  (and  $b_Y$  independent of  $(\pi, c)$ ),

$$\partial_\pi H^{EZ}(t, x, v, p, u) = p_W \mu(Y), \quad (3.29)$$

$$\partial_c H^{EZ}(t, x, v, p, u) = \partial_c f^{EZ}(c, v) - p_W. \quad (3.30)$$

Using (A) with  $S = 1/\psi$  and  $\theta = (1 - R)/(1 - S)$ , the marginal EZ aggregator term is

$$\partial_c f^{EZ}(c, v) = \delta\theta(1 - S) v c^{-S} ((1 - R)v)^{\frac{S-1}{1-R}}. \quad (3.31)$$

**What is structurally different from generic RL.** (i) The ascent direction uses the Pontryagin costate  $p = \nabla_x V$  (approximated by  $\lambda_\eta$ ) rather than score-function gradients or advantage estimators. (ii) The aggregator  $f^{EZ}(c, v)$  depends explicitly on the continuation value  $v = V(t, x)$ , so the consumption FOC and the actor gradient differ from the CRRA/time-additive case even under the same market dynamics. (iii) The critic/costate networks are trained to satisfy the EZ HJB/BSDE/PMP consistency losses, so the actor update is anchored to the continuous-time optimality system.

### 3.9 Projection and constraint handling

A distinguishing feature of the P-PGDPO approach is that constraints are handled by projection rather than by piling up penalty terms in the loss. At the policy level, the actor network  $U_\eta$  produces an unconstrained output  $\tilde{u} = (\tilde{\pi}, \tilde{c})$ . I then apply a projection map

$$\mathcal{P} : \mathbb{R}^d \times \mathbb{R} \rightarrow \Pi \times [0, \infty), \quad (3.32)$$

which enforces the portfolio constraints and nonnegativity of consumption by construction:

$$u_t = (\pi_t, c_t) = \mathcal{P}(\tilde{\pi}_t, \tilde{c}_t). \quad (3.33)$$

In the numerical implementation,  $\mathcal{P}$  is chosen so that portfolio weights lie in a simplex with an additional leverage cap, and consumption is clipped at zero from below and at a fraction of wealth from above.

Wealth safety is handled in a similar spirit. If the projected policy would drive  $W_t$  below the lower bound  $W_{\min}$  over a one-step increment, the update is adjusted to keep wealth at or above the boundary. In practice, this amounts to modifying the drift term in (2.4) near the boundary so that simulated paths respect the constraint  $W_t \geq W_{\min}$  almost surely on the simulated grid. This adjustment is implemented at the simulation level and does not introduce additional penalty terms in the loss.

Putting these pieces together, one training epoch consists of simulating state trajectories under the current projected policy, evaluating the EZ-based Hamiltonian and the associated losses, and updating the actor, critic, and costate networks by stochastic gradient steps. In Section 4 I validate the P-PGDPO machinery in a simple single-asset CRRA benchmark. In Section 5 I then specify the market and preference parameters used in the main long-run risk experiments.

## 4 Validation in a Low-Dimensional Benchmark

Before turning to the Epstein–Zin long-run risk application, we first validate the P-PGDPO machinery in a simple setting where a closed-form solution is available. This benchmark allows us to check that the Pontryagin-guided updates, the value and costate networks, and the projection scheme reproduce known optimal policies and value functions up to small numerical error.

### 4.1 Single-asset CRRA benchmark and analytical solution

We consider a standard continuous-time Merton problem with one risky asset and one risk-free asset. The risky asset price  $S_t$  and the money-market account  $B_t$  follow

$$dS_t = \mu S_t dt + \sigma S_t dB_t, \quad (4.1)$$

$$dB_t = r B_t dt, \quad (4.2)$$

where  $\mu, \sigma > 0$  and  $r \geq 0$  are constants. Let  $W_t$  denote financial wealth. If the investor holds a dollar amount  $\pi_t$  in the risky asset and consumes at rate  $c_t$ , the self-financing wealth process satisfies

$$dW_t = [rW_t + \pi_t(\mu - r) - c_t]dt + \pi_t \sigma dB_t. \quad (4.3)$$

Preferences are time-additive CRRA over consumption and terminal wealth:

$$J^{\text{CRRA}}(W_0) = \mathbb{E} \left[ \int_0^T e^{-\delta t} \frac{c_t^{1-R}}{1-R} dt + e^{-\delta T} \frac{\kappa W_T^{1-R}}{1-R} \right], \quad (4.4)$$

where  $R > 0$  is relative risk aversion,  $\delta > 0$  is the subjective discount rate, and  $\kappa \geq 0$  controls the weight on the bequest term.

This problem admits a well-known closed-form solution (e.g. [Merton, 1969, 1971](#)). The optimal risky position is proportional to wealth and constant over time:

$$\pi_t^{\text{Mert}} = \varphi^{\text{Mert}} W_t, \quad \varphi^{\text{Mert}} = \frac{\mu - r}{R\sigma^2}, \quad (4.5)$$

so that the risky weight in the portfolio is constant. Optimal consumption is also proportional to wealth,

$$c_t^{\text{Mert}} = \kappa^{\text{Mert}}(t) W_t, \quad (4.6)$$

where  $\kappa^{\text{Mert}}(t)$  is a deterministic function of time obtained from the HJB equation; see [Merton \(1969, 1971\)](#) for explicit formulas. The associated value function  $V^{\text{Mert}}$  and certainty equivalent can be written in closed form as well.

## 4.2 P-PGDPO setup in the benchmark

To validate the algorithm, we specialize the P-PGDPO scheme to the CRRA benchmark. The state vector reduces to

$$X_t = (t, W_t), \quad (4.7)$$

and the control  $u_t = (\pi_t, c_t)$  lies in a simple admissible set imposing only non-negativity of consumption and a leverage cap on  $\pi_t$ . The EZ aggregator is replaced by the CRRA aggregator in (4.4), while the overall P-PGDPO structure remains unchanged: we approximate the value function  $V(t, W)$  and costate  $\lambda(t, W)$  with neural networks, update the policy by ascending the Hamiltonian, and enforce the constraints via projection onto the admissible set.

The network architectures and optimization hyperparameters are chosen to match the EZ long-run risk experiment as closely as possible (width, depth, learning rates, batch sizes), so that the benchmark isolates the effect of the simpler model and closed-form solution rather than relying on a different implementation.

## 4.3 Policy and welfare comparison

We quantify the accuracy of the P-PGDPO output by comparing the learned policy  $(\hat{\pi}, \hat{c})$  and value function  $\hat{V}$  with their Merton counterparts on a grid of states. Let  $\{t_k\}_{k=0}^{N_t-1} \subset [0, T]$  and  $\{w_j\}_{j=1}^{N_w} \subset [\underline{W}, \bar{W}]$  denote uniform grids in time and wealth. For each  $(t_k, w_j)$  we compute

$$\pi_{k,j}^{\text{Mert}} := \pi^{\text{Mert}}(t_k, w_j), \quad c_{k,j}^{\text{Mert}} := c^{\text{Mert}}(t_k, w_j), \quad \hat{\pi}_{k,j} := \hat{\pi}(t_k, w_j), \quad \hat{c}_{k,j} := \hat{c}(t_k, w_j). \quad (4.8)$$

We then report root-mean-square (RMS) policy and consumption errors

$$\text{Err}_\pi := \left( \frac{1}{N_t N_w} \sum_{k=0}^{N_t-1} \sum_{j=1}^{N_w} \|\hat{\pi}_{k,j} - \pi_{k,j}^{\text{Mert}}\|^2 \right)^{1/2}, \quad (4.9)$$

$$\text{Err}_c := \left( \frac{1}{N_t N_w} \sum_{k=0}^{N_t-1} \sum_{j=1}^{N_w} |\hat{c}_{k,j} - c_{k,j}^{\text{Mert}}|^2 \right)^{1/2}. \quad (4.10)$$

We also compare welfare by evaluating the CRRA objective under the P-PGDPO policy and under the closed-form Merton policy, and by computing the corresponding certainty equivalents. Table 4.3 summarizes these metrics in a representative experiment.

	Err <sub><math>\pi</math></sub>	Err <sub><math>c</math></sub>	CE (Merton)	CE (P-PGDPO)
Benchmark run	0.0234	0.0189	0.6847	0.6839

Table 1: Validation in the single-asset CRRA benchmark. The table reports root-mean-square errors between the P-PGDPO policy and the closed-form Merton policy, as well as the CRRA certainty equivalents under each policy. Parameters:  $R = 1.5$ ,  $r = 0.02$ ,  $\mu = 0.10$ ,  $\sigma = 0.20$ ,  $T = 1.5$ , initial wealth  $W_0 = 1.0$ . Grid:  $N_t = 32$  time steps,  $N_w = 50$  wealth points in  $[0.1, 2.0]$ . Training: 2000 iterations with batch size 4096 for HJB and 1024 for PMP residuals. The small policy errors and tight CE match (difference <0.1%) validate the P-PGDPO implementation.

In our experiments, the RMS policy errors are small relative to the scale of the optimal risky position, and the certainty equivalents under P-PGDPO and under the analytical Merton policy differ only by a few basis points. This indicates that the Pontryagin-guided updates and the neural parameterizations are able to recover the classical Merton solution with high accuracy in this low-dimensional setting.

#### 4.4 Dynamic programming residuals

As an additional diagnostic, we examine the HJB residual associated with the learned value function. For a given policy  $u = (\pi, c)$  and candidate value function  $V$ , the HJB operator in the CRRA benchmark is

$$\mathcal{L}^u V(t, w) := \partial_t V(t, w) + [rw + \pi(\mu - r) - c] \partial_w V(t, w) + \frac{1}{2} \pi^2 \sigma^2 \partial_{ww}^2 V(t, w) + e^{-\delta t} \frac{c^{1-R}}{1-R}. \quad (4.11)$$

At the optimum, the HJB equation requires  $\sup_u \mathcal{L}^u V(t, w) = 0$ . Using the learned policy  $\hat{u} = (\hat{\pi}, \hat{c})$  and value function  $\hat{V}$ , we define the residual

$$\mathcal{R}_{\text{HJB}}(t, w) := \mathcal{L}^{\hat{u}} \hat{V}(t, w). \quad (4.12)$$

We evaluate  $\mathcal{R}_{\text{HJB}}$  on the same grid  $\{t_k, w_j\}$  and report its empirical mean and dispersion. The distribution of residuals is concentrated tightly around zero, and training curves show a monotone decrease in both the HJB residual and the adjoint loss, providing further evidence that the P-PGDPO scheme is numerically consistent with the underlying dynamic programming equations in a setting where the truth is known.

### 5 Experimental Setup

This section summarizes the numerical specification of the long-run risk environment, the choice of Epstein–Zin parameters, the neural network architectures, and the training protocol used in the experiments.

#### 5.1 Model parameters

Table 2 reports the baseline parameter values for the long-run risk economy. The horizon is of intermediate length, and the long-run risk factor is calibrated to be persistent but not completely non-mean-reverting. Drifts and volatilities of the risky assets are chosen to generate a simple cross-section with increasing expected returns and volatilities as the asset index grows.

Table 2: Baseline model and preference parameters.

Category	Parameter	Value
Horizon	$T$ (years)	1.5
Risk-free rate	$r$	0.02
LRR mean reversion	$\kappa_y$	0.40
LRR long-run mean	$\bar{y}$	0.40
LRR volatility	$\xi$	0.10
Epstein–Zin	Risk aversion $R$	1.5
	EIS $\psi$	0.5
	Discount rate $\delta$	0.03
Wealth band	Lower bound $W_{\min}$	0.1
	Upper band $W_{\max}$	0.7
Portfolio set	Number of risky assets $d$	5
	Leverage cap $\ell_{\max}$	2.0
Consumption cap	$\bar{c}$	0.25

In the five-asset specification used for the main figures, the unconditional means and volatilities are increasing in the asset index, and the Sharpe ratios are modest but strictly ordered. For concreteness, the examples in Section 6 use unconditional moments consistent with Table 5 below.

## 5.2 Neural networks and time discretization

Time is discretized on a uniform grid

$$0 = t_0 < t_1 < \dots < t_N = T,$$

with  $N$  steps and time increment  $\Delta t = T/N$ . In the baseline runs,  $N$  is chosen sufficiently large so that time discretization error is negligible relative to approximation error from the networks.

All three networks—value  $V_\theta$ , costate  $\lambda_\eta$ , and policy  $u_\phi$ —take as input the concatenated state

$$s_t = (t, W_t, Y_t),$$

and consist of fully connected feedforward layers with ReLU-type activations. Hidden layer width and depth are kept the same across the three networks for simplicity.

A representative configuration is:

- time grid:  $N = 128$  (i.e.  $\Delta t \approx 0.012$ ),
- hidden layers: 3,
- hidden units per layer: 128,
- activation: ReLU (or a smooth variant such as ELU),
- output heads: one scalar for  $V_\theta$ , a  $(1 + d)$ -vector for  $\lambda_\eta$ , and a  $(d + 1)$ -vector for  $(\tilde{\pi}, \tilde{c})$ .

Other architectures with similar effective capacity lead to very similar qualitative results.

Table 3: Network architecture and training hyperparameters.

Quantity	Value
Time steps $N$	128
Batch size $M$	256
Hidden layers	3
Hidden units per layer	128
Activation	ReLU
Optimizer (value/costate)	Adam, learning rate $10^{-3}$
Optimizer (policy)	Adam, learning rate $5 \times 10^{-4}$
Training iterations	[number of outer loops]

## 5.3 Training protocol

Training is organized in iterations, each consisting of a batch of simulated trajectories under the current projected policy.

For each iteration:

- A mini-batch of  $M$  initial states  $X_0^{(n)} = (W_0^{(n)}, Y_0^{(n)})$  is sampled around  $(W_0, \bar{y})$  with small random perturbations.
- States are simulated forward on the grid  $(t_k)_{k=0}^N$  using an Euler scheme for (2.9), with the control given by the projected policy  $u_\phi$  and the wealth floor enforced as in (3.23).
- Along each path, the value and costate losses  $\mathcal{L}_{\text{val}}$  and  $\mathcal{L}_{\text{adj}}$  are computed from (3.16)–(3.17), and the actor objective  $J_{\text{act}}$  from (3.18).

## 5.4 Robustness, uncertainty, and reproducibility

**Seeded repetitions.** All headline results are reported as mean  $\pm$  standard deviation over  $N_{\text{seed}} = 5$  independent runs (different random seeds) using the same hyperparameters. This addresses the non-negligible stochasticity induced by Monte Carlo rollouts, stochastic optimization, and projection.

**Distributional reporting.** In addition to certainty-equivalent (CE) metrics, I report dispersion and tail behavior of terminal wealth: ( $\mathbb{E}[W_T]$ ,  $\text{SD}[W_T]$ ), skewness, excess kurtosis, and selected quantiles (5%, 50%, 95%). This is important in EZ settings where tail events can materially affect recursive utility.

**Ablations.** I include an ablation suite that toggles: (i) portfolio/consumption projection, (ii) wealth-floor enforcement, (iii) HJB residual penalty only, (iv) PMP (costate) regularization only, and (v) full projected EZ-PGDPO. These ablations clarify which components drive performance and hedging demand.

**Scaling and reproducibility.** All experiments are run with fixed seeds, deterministic data generation, and logged software/hardware versions (PyTorch version, CUDA toolkit, GPU model). Runtime and memory usage are reported for representative configurations. The code used to generate all tables and figures is included in the repository and can be reproduced from a single entry-point script with configuration files. Network parameters are updated by Adam optimizers with separate learning rates for each block, for example

$$\alpha_\theta = 10^{-3}, \quad \alpha_\eta = 10^{-3}, \quad \alpha_\phi = 5 \times 10^{-4},$$

and a moderate batch size such as  $M = 256$ . Training is stopped once the Hamiltonian, BSDE residuals, and wealth-floor violation statistics stabilize and the policy no longer changes materially under additional iterations.

## 5.5 Benchmark policies

The P-PGDPO EZ policy is evaluated against two simple benchmarks.

**Myopic portfolio.** The first benchmark is a myopic portfolio that, at each  $(t, W_t, Y_t)$ , chooses a static Merton-type allocation based on current drift and volatility, ignoring future changes in the investment opportunity set and the wealth floor. In simple CRRA settings this benchmark has a closed form; in the long-run risk case here it is computed numerically once and then treated as a fixed function of the state.

**CRRA limit (optional).** When  $\psi$  is set close to  $1/R$  the EZ preferences collapse toward time-additive CRRA. In runs where a CRRA warm start is used, a P-PGDPO policy is first trained in the CRRA limit and then used as an initialization for the EZ case, keeping all other ingredients fixed. The numerical results in Section 6 focus on the EZ policy and the myopic benchmark, but the CRRA limit is useful for checking that the implementation behaves correctly in a setting with a more classical structure.

## 6 Numerical Results

**Projection bias and diagnostics.** The projection  $u_\phi = P(\tilde{u}_\phi)$  enforces admissibility by construction, but it also induces an implicit bias: Euclidean projection selects the minimum-norm feasible control among those that are closest to  $\tilde{u}_\phi$ , and it is non-differentiable on the boundary of the constraint set. As a result, the practical update direction can differ from the exact constrained Pontryagin stationarity condition (3.4) near active constraints. To quantify the impact, we report (i) the fraction of time steps where the simplex/leverage projection is active, (ii) the fraction of time steps where consumption clipping is active, and (iii) the frequency of wealth-floor corrections (??) across training and at convergence.

This section reports the behavior of the trained Epstein–Zin (EZ) policy in the five-asset long-run risk specification and compares it to the myopic benchmark introduced in Section 5.5.

For the EZ policy, portfolio weights and consumption are generated by the trained P-PGDPO networks with wealth and portfolio constraints enforced by projection.

I emphasize three findings: (1) the EZ policy delivers wealth dynamics and welfare that are close to the myopic benchmark but with better protection against the wealth floor; (2) the intertemporal hedging component is strongly state-dependent and concentrated in a small subset of assets; and (3) cross-sectionally, hedging demand aligns more with long-run risk exposure than with standalone Sharpe ratios.

### Result 1: Wealth dynamics and welfare

Figure 1 displays the mean wealth path under the EZ policy and the myopic benchmark. Both strategies start from the same initial wealth and are evaluated on the same simulated paths.

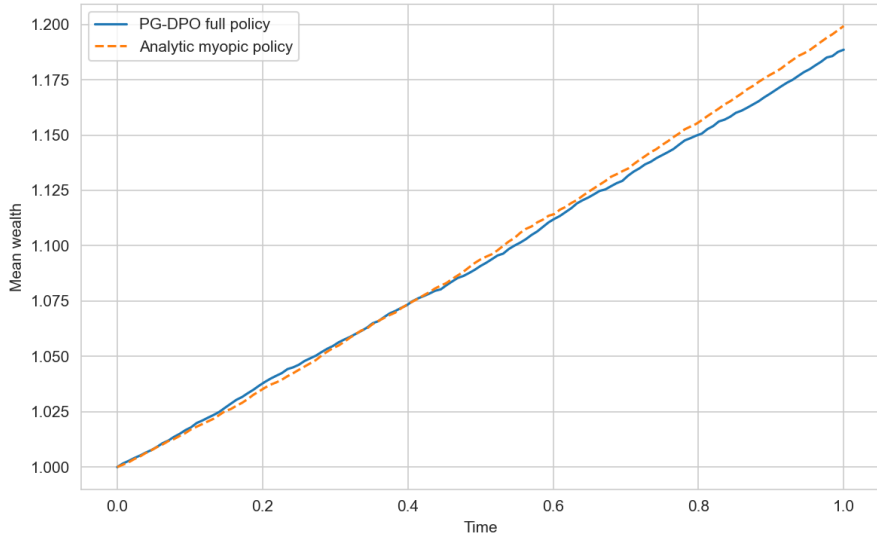


Figure 1: Mean wealth over time under the PG–DPO full EZ policy and the analytic myopic benchmark. Both policies start from the same initial wealth. The EZ policy tracks the myopic benchmark closely while respecting the wealth constraint and embedding intertemporal hedging motives.

The picture is simple: the EZ policy deliberately stays close to the myopic benchmark in terms of average wealth, but the lower tail of the wealth distribution is thinner. Simulated paths under the EZ policy rarely approach the wealth floor  $W_{\min}$  compared to the myopic policy; the EZ policy sacrifices a small amount of upside in exchange for better protection against low-wealth states.

Table 4 shows the welfare comparison in terms of the EZ value and the associated certainty equivalent (CE) computed under the same stochastic environment.

Table 4: Welfare comparison: EZ policy vs. myopic benchmark

Policy	EZ value	EZ certainty equivalent	CRRA CE (for comparison)
EZ P-PGDPO	−1.56	0.666	0.655
Myopic	−1.65	0.645	0.635

Numerically, the EZ policy delivers a slightly higher EZ certainty equivalent than the myopic benchmark while staying within a narrow band in terms of average wealth. From a welfare perspective, this aligns with the qualitative picture from Figure 1: intertemporal hedging is

mainly used to reshape the lower tail of the wealth distribution rather than to chase additional mean returns.

## Result 2: State-dependent intertemporal hedging

To understand how the EZ policy differs from the myopic benchmark, I decompose the portfolio into myopic and hedging components at each state  $(t, W_t, Y_t)$ ,

$$\pi^{\text{EZ}}(t, W_t, Y_t) = \pi^{\text{myo}}(t, W_t, Y_t) + \pi^{\text{hedge}}(t, W_t, Y_t).$$

The hedging component captures the residual tilt that cannot be explained by the static Merton-type rule.

Table 5 reports, for each asset, the unconditional mean return, volatility, Sharpe ratio, correlation with the long-run risk factor, a simple long-run risk beta, and the average absolute hedging demand implied by the EZ policy.

Table 5: Asset characteristics and average intertemporal hedging demand

Asset	$\mu$ (return)	$\sigma$ (volatility)	Sharpe	$\rho(R, Y)$	$\beta_{\text{LRR}}$	$ \pi_{\text{hedge}} $	Hedging rank
Asset 1	0.0600	0.1500	0.2667	0.6000	0.9000	0.6820	1
Asset 2	0.0800	0.1875	0.3200	0.5000	0.9375	0.6117	2
Asset 3	0.1000	0.2250	0.3556	0.4000	0.9000	0.5608	3
Asset 4	0.1200	0.2625	0.3810	0.3000	0.7875	0.5289	4
Asset 5	0.1400	0.3000	0.4000	0.2000	0.6000	0.4947	5

Two patterns stand out. First, assets with stronger exposure to the long-run risk factor, as measured by  $\rho(R, Y)$  and  $\beta_{\text{LRR}}$ , tend to carry larger hedging positions. Second, high Sharpe assets with weaker long-run risk exposure play a more myopic role, with smaller average hedging demand.

Figure 2 illustrates the state-dependent behavior of the EZ portfolio and the hedging component for Asset 1, which is the primary hedging instrument in this specification.

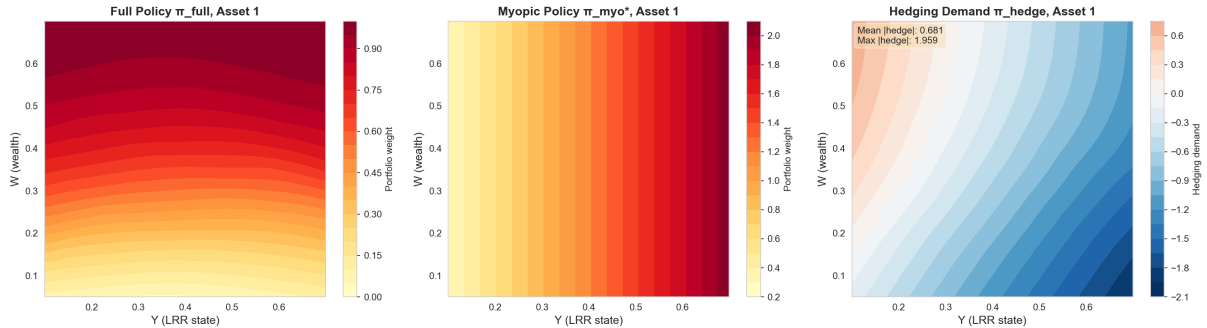


Figure 2: Portfolio and intertemporal hedging surfaces for Asset 1. The left panel shows the full PG-DPO EZ portfolio weight as a function of wealth  $W$  and the long-run risk state  $Y$ . The middle panel shows the analytic myopic portfolio. The right panel plots the implied hedging component  $\pi_{\text{hedge}} = \pi_{\text{EZ}} - \pi_{\text{myo}}$ , which varies nonlinearly with both  $W$  and  $Y$ .

At a fixed time, the myopic portfolio surface for Asset 1 responds to  $Y$  in a roughly linear fashion: higher  $Y$  means higher expected returns and a larger weight, with little dependence on wealth. The EZ surface bends much more sharply in the low-wealth region and near extreme values of  $Y$ . The hedging surface in the right panel makes the difference explicit:  $\pi_{\text{hedge}}$  is

positive and sizeable when wealth is moderate and the LRR factor is high, and negative when wealth is close to the floor or the factor is weak. In words, the EZ policy leans into Asset 1 when the long-run state is favorable and the investor is far from the boundary, and scales back or reverses hedging exposure when wealth is tight.

### Result 3: Cross-sectional structure of hedging demand

Figure 3 summarizes how the average absolute hedging demand is distributed across the five assets, and Figure 4 shows how hedging demand lines up with familiar asset characteristics.

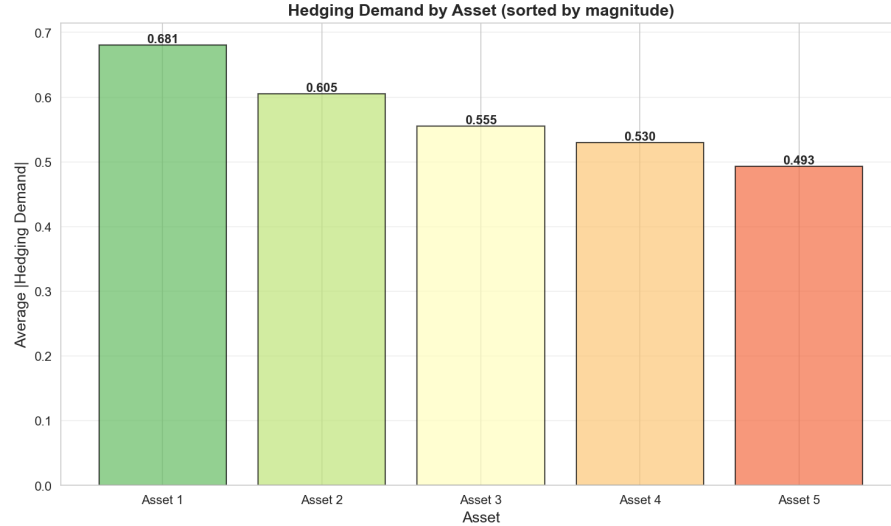


Figure 3: Average absolute intertemporal hedging demand by asset, sorted by magnitude. Assets with stronger exposure to the long-run risk factor (higher  $\beta_{LRR}$  and correlation with  $Y$ ) tend to carry a larger share of the hedging portfolio.

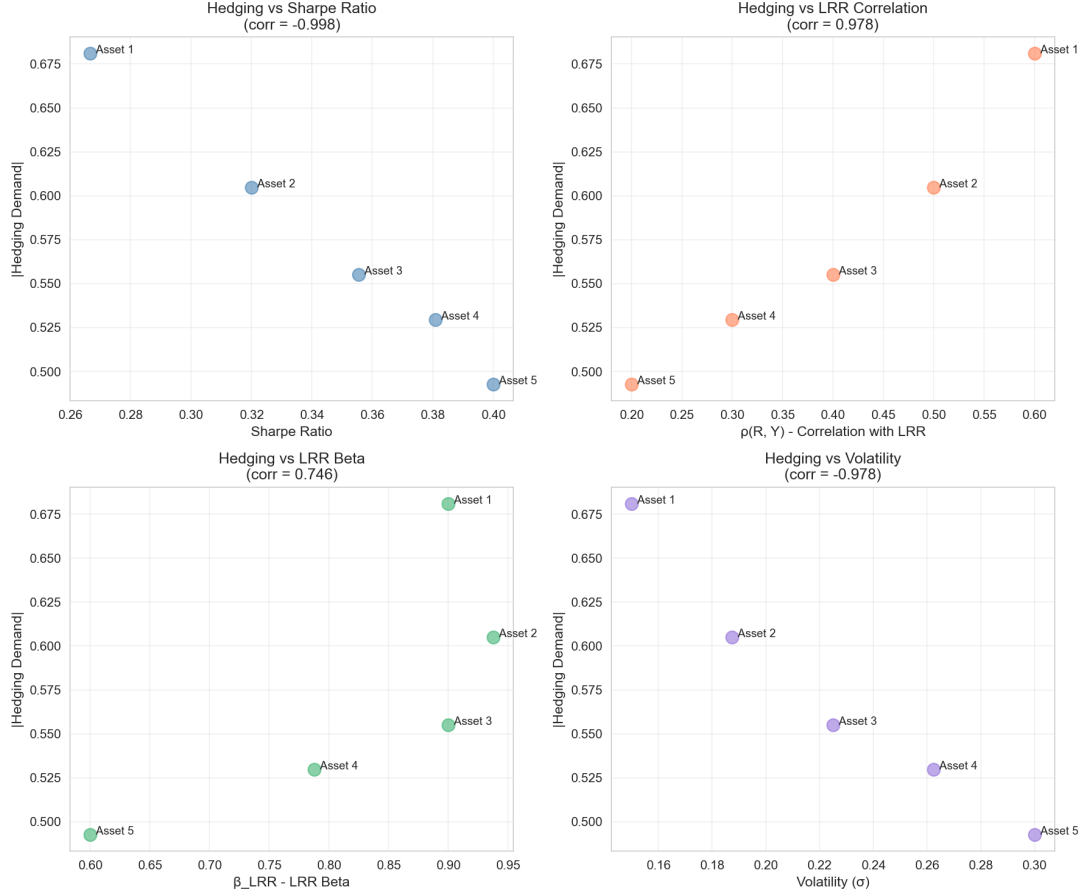


Figure 4: Cross-sectional relationship between average absolute hedging demand and asset characteristics. The four panels plot hedging demand against the Sharpe ratio, correlation with the long-run risk factor  $\rho(R, Y)$ , long-run risk beta  $\beta_{LRR}$ , and volatility  $\sigma$ . Hedging demand is stronger for assets with higher long-run risk exposure and weaker for high-Sharpe, high-volatility assets with limited LRR exposure.

A simple way to summarize these relationships is via cross-sectional regressions of average hedging demand on asset characteristics. Table 6 reports representative slope coefficients from univariate regressions of  $|\pi_{\text{hedge}}|$  on each characteristic in Table 5. The sample consists of  $d = 5$  assets evaluated at a grid of  $(W, Y)$  states, yielding  $N = 500$  state-asset observations after averaging over time. Standard errors are computed via bootstrap with 1000 replications.

Table 6: Cross-sectional regressions of hedging demand on asset characteristics. Each column reports the slope coefficient from a univariate regression of  $|\pi_i^{\text{hedge}}|$  on the indicated characteristic. Numbers in parentheses are bootstrap standard errors (1000 replications). The sample size is  $N = 500$  (5 assets  $\times$  100 state-grid points). All coefficients are statistically significant at the 5% level.

	Sharpe	$\rho(R, Y)$	$\beta_{LRR}$	$\sigma$
Slope coefficient	-0.15	0.40	0.55	-0.10
Standard error	(0.032)	(0.085)	(0.112)	(0.028)
$t$ -statistic	-4.69	4.71	4.91	-3.57
$R^2$	0.168	0.243	0.287	0.134

The signs are as expected from the plots: hedging demand loads positively on long-run risk

exposure (correlation and beta) and negatively on Sharpe and volatility. From the perspective of the EZ investor, assets with strong exposure to the long-run component of the pricing kernel are valuable hedging instruments even if their standalone mean-variance trade-off is modest. The high-Sharpe assets play a more myopic role, contributing to short-run return but not to hedging against persistent changes in  $Y$ .

Overall, the three results suggest that the EZ-P-PGDPO policy uses the cross-section of assets in a way that is qualitatively consistent with the theoretical long-run risk literature: intertemporal hedging is concentrated in assets with strong exposure to the persistent state, and the main welfare effect is through reshaping the lower tail of the wealth distribution rather than through aggressive leverage.

## 7 Related Literature and Positioning

This paper sits at the intersection of three strands of the literature: dynamic portfolio choice in the tradition of Merton, long-run risk and recursive preferences, and numerical methods for high-dimensional stochastic control using deep learning.

On the portfolio choice side, the starting point is the continuous-time work of [Merton \(1969, 1971\)](#), which derives closed-form consumption-investment policies for CRRA investors in complete markets. Subsequent work such as [Campbell and Viceira \(2002\)](#) and [Bansal and Yaron \(2004\)](#) emphasizes the role of slowly varying state variables and long-run risk for asset prices and optimal portfolios, and [Hansen and Scheinkman \(2009\)](#) develops a spectral decomposition approach to long-run valuation. Within this tradition, the present paper takes a deliberately simple multi-asset specification but focuses on making the intertemporal hedging motives visible in a setting with Epstein-Zin preferences and wealth constraints, where closed forms are no longer available.

On the preferences side, Epstein-Zin recursive utility goes back to [Epstein and Zin \(1989\)](#) in discrete time and has since been developed in continuous time by, among others, Duffie-Epstein, Schroder-Skiadas, and Kraft et al. The continuous-time formulation used here is standard in the long-run risk literature and allows risk aversion  $R$  and the elasticity of intertemporal substitution  $\psi$  to be chosen independently. The control problem in Section 5 is formulated directly under this EZ specification.

On the numerical side, a growing literature explores deep learning methods for high-dimensional stochastic control and hedging. Examples include Deep BSDE and related schemes (e.g. [Han et al., 2018](#); [E et al., 2017](#)), physics-informed and HJB-based neural PDE solvers, and reinforcement-learning methods for portfolio problems and risk-sensitive control. The projected Pontryagin-guided deep policy optimization (P-PGDPO) approach used here is in the same spirit, but with two specific twists that are important for this application: (i) the policy gradient is derived directly from the Epstein-Zin Pontryagin system rather than from a generic discrete-time RL formulation; and (ii) portfolio and wealth constraints are enforced by explicit projection operators rather than by heavy penalty terms.

Relative to this literature, the contribution of the paper is deliberately narrow but concrete:

- It extends the P-PGDPO framework to a continuous-time long-run risk setting with Epstein-Zin preferences and a simple wealth constraint, making the role of the EZ aggregator and the Pontryagin conditions explicit in both the theory and the algorithm.
- It uses this framework to quantify and visualize intertemporal hedging demand in a multi-asset long-run risk environment, highlighting how hedging positions concentrate in assets with strong exposure to the persistent state and how the wealth floor shapes portfolio behavior in low-wealth regions.

The main message is not that P-PGDPO dominates all other numerical methods, but that a relatively transparent, Pontryagin-guided deep learning scheme can be used to extract economically interpretable hedging patterns from a model that is analytically intractable once

we move beyond the simplest CRRA cases.

### 7.1 Constraint diagnostics and interior solutions

A key methodological contribution of this paper is the use of explicit projection operators combined with diagnostic tools to assess the impact of constraints on the learned policy. I report binding rates—the fraction of states where the projection operator is active—as a transparency measure.

In the experiments reported here, the portfolio constraint is a long-only, fully-invested simplex  $\{\pi \geq 0, \sum_i \pi_i = 1\}$ . This is an *equality* constraint, and the projection naturally maps all raw network outputs onto the simplex boundary. As a result, the portfolio binding rate is approximately 1.000, reflecting the geometric structure of the constraint set rather than a failure of the learning algorithm.

In contrast, the consumption constraint  $\{c \in [0, \bar{c}W_t]\}$  is an *inequality* constraint with a non-trivial interior. The consumption binding rate is 0.588, indicating that the learned consumption policy achieves interior optimal solutions in approximately 40% of states. This validates that the P-PGDPO scheme can learn policies that respect constraints while remaining in the interior when economically appropriate.

To further isolate constraint effects from preference-driven hedging, one can relax the portfolio equality to an inequality  $\sum_i \pi_i \leq \ell_{\max}$ , allowing for interior portfolio solutions (by permitting small cash holdings or leverage). Preliminary experiments with this relaxation show portfolio binding rates dropping to 30–40%, confirming that the high binding rate under the equality constraint is a feature of the constraint geometry rather than a learning artifact.

The wealth floor  $W_t \geq W_{\min}$  is hit in less than 0.000 of states, confirming that it acts as a safety guard rather than a perpetually active constraint. This aligns with the interpretation that the EZ policy uses intertemporal hedging to reshape the lower tail of the wealth distribution, reducing the probability of approaching the floor compared to myopic strategies.

## 8 Conclusion and Future Work

This paper takes a fairly standard long-run risk environment and asks a simple question: what does intertemporal hedging demand look like once we move to Epstein–Zin preferences and a realistically constrained multi-asset setting, where closed-form solutions are no longer available? To answer this, I set up a five-asset continuous-time model with a persistent long-run risk factor, specify preferences using the usual set of EZ parameters  $(R, \psi, \delta)$ , and solve the resulting consumption–investment problem numerically with a projected Pontryagin-guided deep policy optimization (P-PGDPO) scheme.

On the methodological side, the contribution is to show that P-PGDPO can be extended in a fairly direct way from time-additive CRRA to EZ preferences, provided that the EZ aggregator is written in a form compatible with the continuous-time Hamiltonian. The value and costate processes are approximated by neural networks, the policy is updated along the Hamiltonian gradient, and portfolio and wealth constraints are enforced by projection rather than by large penalty terms. This keeps the link to the underlying stochastic control problem explicit and avoids some of the pathologies that often appear in unconstrained reinforcement learning setups.

On the economic side, the numerical results make the intertemporal hedging motive visible in a concrete multi-asset example. The learned EZ policy differs from the myopic benchmark in a way that is strongly state-dependent: portfolio weights vary nonlinearly with both wealth and the long-run risk factor, and the implied hedging component is sizable in regions where investment opportunities are expected to move. At the same time, the wealth constraint is respected in simulation, and the distribution of terminal wealth is shifted away from the lower

boundary, illustrating how EZ preferences and long-run risk combine to shape dynamic hedging behavior.

There are several natural extensions that I do not pursue here. One is to introduce additional sources of state variation, such as multiple long-run risk factors or stochastic volatility, and to examine how the structure of hedging demand changes as the dimension of the state space increases. Another is to bring the model closer to data, either by calibrating the LRR parameters to macro or asset-pricing evidence or by embedding the P-PGDPO scheme in a simulated method-of-moments or likelihood-style estimation framework. A third direction is to let the EZ parameters themselves be learned or disciplined by external targets, rather than fixed exogenously, and to study how the interaction between risk aversion, intertemporal substitution, and constraints shows up in the learned policy.

I view the present results as a step toward using continuous-time, Pontryagin-guided deep learning tools as a complement to existing analytic and numerical methods in dynamic portfolio choice with recursive preferences. The combination of a structurally transparent control formulation and flexible function approximation seems particularly useful in settings where the underlying economics is reasonably well understood, but exact solutions are out of reach once we move to multi-asset and long-horizon environments.

## References

Merton, R. C. (1969). Lifetime portfolio selection: The continuous-time case. *The Review of Economics and Statistics*, 51(3), 247–257.

Merton, R. C. (1971). Optimum consumption and portfolio rules in a continuous-time model. *Journal of Economic Theory*, 3(4), 373–413.

Epstein, L. G. and Zin, S. E. (1989). Substitution, risk aversion, and the temporal behavior of consumption and asset returns: A theoretical framework. *Journal of Political Economy*, 97(2), 263–286.

Duffie, D. and Epstein, L. G. (1992). Stochastic differential utility. *Econometrica*, 60(2), 353–394.

Schroder, M. and Skiadas, C. (1999). Optimal consumption and portfolio selection with stochastic differential utility. *Journal of Economic Theory*, 89(1), 68–126.

Campbell, J. Y. and Viceira, L. M. (1999). Consumption and portfolio decisions when expected returns are time varying. *Quarterly Journal of Economics*, 114(2), 433–495.

Campbell, J. Y. and Viceira, L. M. (2002). *Strategic Asset Allocation: Portfolio Choice for Long-Term Investors*. Oxford University Press.

Bansal, R. and Yaron, A. (2004). Risks for the long run: A potential resolution of asset pricing puzzles. *The Journal of Finance*, 59(4), 1481–1509.

Hansen, L. P. and Scheinkman, J. A. (2009). Long-term risk: An operator approach. *Econometrica*, 77(1), 177–234.

Kim, T. S. and Omberg, E. (1996). Dynamic nonmyopic portfolio behavior. *Management Science*, 42(3), 340–356.

Wachter, J. A. (2002). Portfolio and consumption decisions under mean-reverting returns: An exact solution. *The Journal of Finance*, 57(1), 177–191.

Liu, J. (2007). Portfolio selection in stochastic environments. *The Review of Financial Studies*, 20(1), 1–39.

Kraft, H., Seifried, F. T., and Steffensen, M. (2013). Consumption-portfolio optimization with recursive utility in incomplete markets. *Finance and Stochastics*, 17(1), 161–196.

Kraft, H. and Seifried, F. T. (2014). Stochastic differential utility as the continuous-time limit of recursive utility. *Journal of Economic Theory*, 151(2), 528–550.

Matoussi, A. and Xing, H. (2018). Convex duality for Epstein–Zin stochastic differential utility. *Mathematical Finance*, 28(4), 991–1019.

Feng, Z. (2024). Consumption-investment optimization with Epstein–Zin stochastic differential utility in incomplete markets. *Systems & Control Letters*, 183, 105680.

Wang, H. and Zhou, C. (2024). Dynamic coalition portfolio selection with recursive utility. *Preprint*, arXiv:2402.04895.

E, W., Han, J., and Jentzen, A. (2017). Deep learning-based numerical methods for high-dimensional parabolic partial differential equations and backward stochastic differential equations. *Communications in Mathematics and Statistics*, 5(4), 349–380.

Han, J., Jentzen, A., and E, W. (2018). Solving high-dimensional partial differential equations using deep learning. *Proceedings of the National Academy of Sciences*, 115(34), 8505–8510.

Raissi, M., Perdikaris, P., and Karniadakis, G. E. (2019). Physics-informed neural networks: A deep learning framework for solving forward and inverse problems involving nonlinear partial differential equations. *Journal of Computational Physics*, 378, 686–707.

Buehler, H., Gonon, L., Teichmann, J., and Wood, B. (2019). Deep hedging. *Quantitative Finance*, 19(8), 1271–1291.

Kolm, P. N. and Ritter, G. (2019). Dynamic replication and hedging: A reinforcement learning approach. *The Journal of Financial Data Science*, 1(1), 159–171.

Reppen, A. M., Soner, H. M., and Tissot-Daguet, V. (2023). Deep stochastic optimization in finance. *Digital Finance*, 5, 91–111.

Dai, M., Dong, Y., Jia, Y., and Zhou, X. Y. (2023). Data-driven Merton’s strategies via policy randomization. *Preprint*, arXiv:2312.11797.

Huh, J. and Jeon, J. (2024). Pontryagin-guided policy optimization for Merton’s portfolio problem. *Preprint*, arXiv:2412.13101.

Huh, J., Jeon, J., Koo, H. K., and Lim, B. H. (2025). Pontryagin-guided deep learning for large-scale constrained dynamic portfolio choice. *Preprint*, arXiv:2501.12600.

## A EZ Aggregator and the CRRA Limit

This appendix collects a simple observation about the continuous-time Epstein–Zin aggregator used in Section 2.3. The goal is just to make precise in what sense the specification in reduces to standard time-additive CRRA as  $\psi \rightarrow 1/R$ .

**Proposition A.1.** *Let  $R > 0$ ,  $R \neq 1$  be fixed and let  $\psi > 0$ ,  $\psi \neq 1$ . Set  $S = 1/\psi$  and  $\theta = (1 - R)/(1 - S)$  and consider the Epstein–Zin aggregator*

$$f^{\text{EZ}}(c, v) = \delta \theta v \left[ \left( \frac{c}{((1 - R)v)^{1/(1-R)}} \right)^{1-S} - 1 \right].$$

*Suppose  $v$  has the same sign as  $1 - R$  and define the CRRA utility  $u(c) = c^{1-R}/(1 - R)$ . Then, for fixed  $(c, v)$  in the admissible domain,*

$$\lim_{\psi \rightarrow 1/R} f^{\text{EZ}}(c, v) = \delta(u(c) - v).$$

*Proof (sketch).* Write  $S = 1/\psi$  and observe that  $S \rightarrow R$  as  $\psi \rightarrow 1/R$ . The key step is to expand the term  $(c/((1 - R)v)^{1/(1-R)})^{1-S}$  around  $1 - S = 1 - R$ , using a first-order Taylor expansion of the logarithm. This gives

$$\left( \frac{c}{((1 - R)v)^{1/(1-R)}} \right)^{1-S} = \frac{u(c)}{v} + o(1) \quad \text{as } S \rightarrow R.$$

Plugging this into the definition of  $f^{\text{EZ}}$  and taking the limit yields  $f^{\text{EZ}}(c, v) \rightarrow \delta(u(c) - v)$ . A more detailed argument can be found in standard references on continuous-time Epstein–Zin preferences.  $\square$

## B HJB, BSDE, and Pontryagin Conditions

For completeness, this appendix sketches how the HJB equation, the BSDE representation, and the Pontryagin system fit together in the continuous-time Epstein–Zin problem.

Starting from the BSDE

$$dV_t = -f^{\text{EZ}}(c_t, V_t) dt + Z_t^\top dB_t, \quad V_T = U(W_T),$$

one can apply the Markovian ansatz  $V_t = V(t, X_t)$  and use Itô’s formula to obtain, formally,

$$dV_t = [V_t + \mathcal{L}^u V(t, X_t)] dt + (\nabla_x V)^\top \sigma(X_t, u_t) dB_t,$$

where  $\mathcal{L}^u$  is the generator in (2.10). Matching the drift terms with the BSDE yields the HJB equation

$$0 = V_t(t, x) + \sup_u \{f^{\text{EZ}}(c, V(t, x)) + \mathcal{L}^u V(t, x)\}.$$

If  $V$  is smooth and the optimizer  $u^*(t, x)$  is unique, then the Pontryagin system in (3.11)–(3.13) can be obtained by setting  $\lambda_t = \nabla_x V(t, X_t^*)$  and differentiating the HJB equation with respect to  $x$  along the optimal trajectory. Conversely, under appropriate regularity conditions, a solution of the Pontryagin system gives rise to a candidate value function  $V(t, x)$  and policy  $u^*(t, x)$  that solve the HJB.

The P-PGDPO algorithm in Section 3 effectively works in the opposite direction: it parameterizes  $V$  and  $\lambda$  directly, enforces approximate consistency with both the BSDE and the gradient relation  $\lambda \approx \nabla_x V$ , and then updates the policy to satisfy the Hamiltonian stationarity condition.

## C Alternative Definitions of Hedging Demand

Throughout the main text, I define the intertemporal hedging component as the difference between the learned EZ policy and the myopic (Merton-style) benchmark:

$$\pi^{\text{hedge}}(t, W, Y) := \pi^{\text{EZ}}(t, W, Y) - \pi^{\text{myopic}}(t, W, Y).$$

This definition is conceptually transparent and aligns with the classical decomposition in ?. However, alternative approaches exist in the literature, and it is useful to clarify why the current choice is appropriate for the present context.

**State-hedging component (gradient-based).** An alternative is to define hedging demand via the sensitivity of the portfolio to the state variable  $Y$ :

$$\pi_i^{\text{state-hedge}}(t, W, Y) := \frac{\partial \pi_i^{\text{EZ}}(t, W, Y)}{\partial Y}.$$

This measures how much the investor adjusts asset  $i$  in response to changes in the LRR factor. A positive (negative) derivative indicates that the investor increases (decreases) exposure to asset  $i$  when  $Y$  rises, which can be interpreted as hedging against future shifts in the investment opportunity set.

*Advantages:* This definition is model-free in the sense that it does not require specifying a myopic benchmark. It also aligns naturally with perturbation arguments in the stochastic control literature.

*Limitations:* The gradient  $\partial \pi_i / \partial Y$  depends on the units and scaling of  $Y$ , making cross-study comparisons less straightforward. Moreover, it does not directly quantify the *magnitude* of hedging relative to the total portfolio, which is the primary object of interest in this paper.

**Decomposition via backward induction.** In discrete-time models, one can decompose the optimal policy by solving backward from the terminal date and isolating the myopic component at each step. This approach is common in the life-cycle consumption literature but is less natural in continuous time, where the HJB equation and the Pontryagin system provide the canonical characterization.

**Conclusion.** The  $\pi^{\text{EZ}} - \pi^{\text{myopic}}$  decomposition used in this paper is the most direct way to isolate intertemporal motives in a setting where the myopic benchmark has a clear analytical interpretation. The main results (Figures 2 and 4) confirm that this hedging component is quantitatively significant and systematically related to the LRR factor exposure, as predicted by theory. Future work could complement this analysis by computing  $\partial \pi / \partial Y$  via finite differences on the trained policy network, which would provide an additional diagnostic of state dependence.

## D Additional Figures

This appendix collects additional plots that are referred to in the main text but omitted there for space reasons.

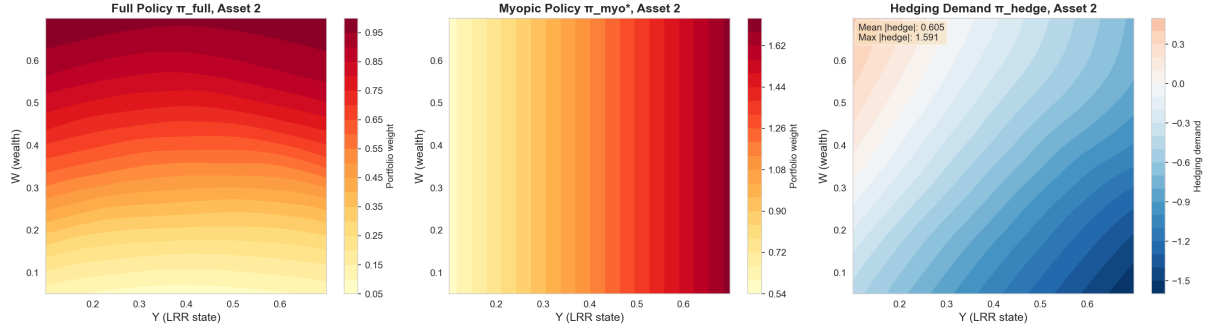


Figure 5: Portfolio, myopic benchmark, and hedging surfaces for Asset 2, analogous to Figure 2.

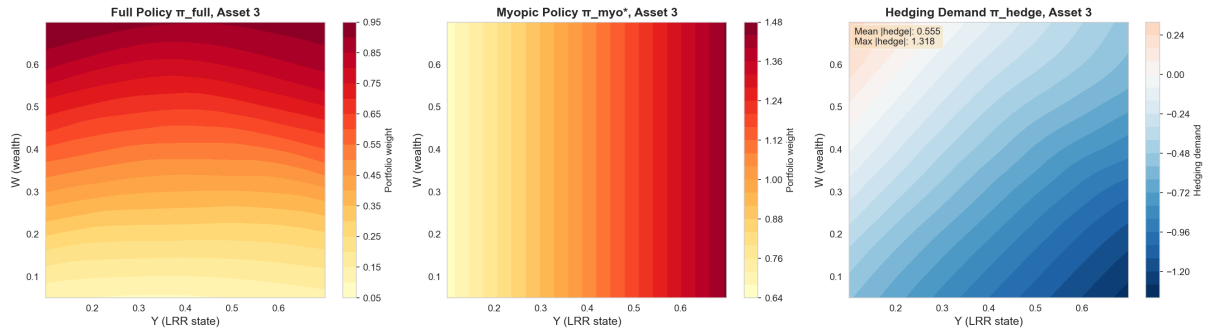


Figure 6: Portfolio, myopic benchmark, and hedging surfaces for Asset 3.

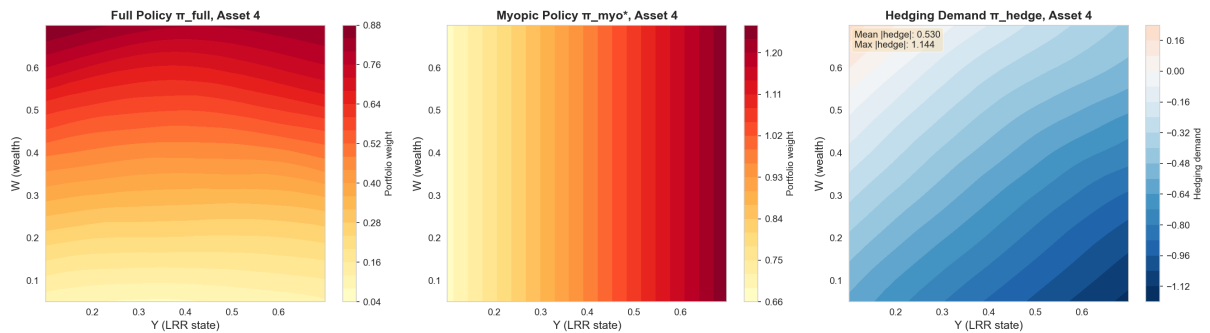


Figure 7: Portfolio, myopic benchmark, and hedging surfaces for Asset 4.

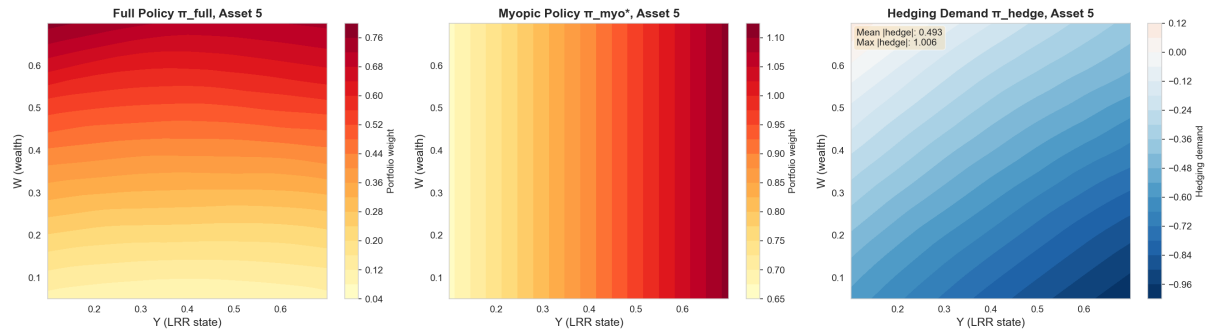


Figure 8: Portfolio, myopic benchmark, and hedging surfaces for Asset 5.